Connectivity reveals relationship of brain areas for reward-guided learning and decision making in human and monkey frontal cortex

Franz-Xaver Neubert[a,1], Rogier B. Mars[a,b,c], Jérôme Sallet[a], and Matthew F. S. Rushworth[a,b]

[a]Department of Experimental Psychology, University of Oxford, Oxford OX1 3UD, United Kingdom and [b]Centre for Functional MRI of the Brain (FMRIB), Nuffield Department of Clinical Neurosciences, John Radcliffe Hospital, Oxford OX3 9DU, United Kingdom; and [c]Donders Institute for Brain, Cognition and Behaviour, Radboud University Nijmegen, 6525 EZ Nijmegen, The Netherlands

Edited by Ranulfo Romo, Universidad Nacional Autonóma de México, Mexico City, D.F., Mexico, and approved February 25, 2015 (received for review June 9, 2014)

Reward-guided decision-making depends on a network of brain regions. Among these are the orbitofrontal and the anterior cingulate cortex. However, it is difficult to ascertain if these areas constitute anatomical and functional unities, and how these areas correspond between monkeys and humans. To address these questions we looked at connectivity profiles of these areas using resting-state functional MRI in 38 humans and 25 macaque monkeys. We sought brain regions in the macaque that resembled 10 human areas identified with decision making and brain regions in the human that resembled six macaque areas identified with decision making. We also used diffusion-weighted MRI to delineate key human orbital and medial frontal brain regions. We identified 21 different regions, many of which could be linked to particular aspects of reward-guided learning, valuation, and decision making, and in many cases we identified areas in the macaque with similar coupling profiles.

orbitofrontal cortex | anterior cingulate cortex | decision making | resting state functional connectivity | comparative anatomy

As humans we make decisions by taking into account different types of information, weighing our options carefully, and eventually coming to a conclusion. We then learn from witnessing the outcome of our decisions. Human functional MRI (fMRI) has had a major impact on elucidating the neural networks mediating decision making and learning, but key insights can only be obtained in neural recording, stimulation, and focal lesion studies conducted in animal models, such as the macaque. Combining insights from human fMRI and animal studies is, however, not straightforward because there is uncertainty about basic issues, such as anatomical and functional correspondences between species (1). For example, although there are many reports of decision value-related activity in the human ventromedial prefrontal cortex (vmPFC) (2, 3), it is unclear whether they can be related to reports of reward-related activity either on the ventromedial surface of the frontal lobe (4, 5), in the adjacent medial orbitofrontal sulcus (6), or indeed to any macaque brain area. It is claimed that some areas implicated in reward-guided decision making and learning, such as parts of anterior cingulate cortex (ACC), are not found in macaques (7), but such theories have never been formally tested.

In addition, there is uncertainty about the basic constituent components of decision-making and learning circuits. To return to the example of the vmPFC, although this region is often contrasted with similarly large subdivisions of the frontal cortex, such as the lateral orbitofrontal cortex (lOFC) and ACC (8), it is unclear whether, and if so how, it should be decomposed into further subdivisions. Moreover, there are sometimes fundamental disagreements about how brain areas contribute to decision making and learning. For example, it has been claimed both that the ACC does (9–11) and does not (12) contribute to reward-based decision making and that it is concerned with distinct processes for task control, error detection, and conflict resolution (13, 14). Reliable identification and location of ACC subcomponent regions could assist the resolution of such debates.

In the present study we formally compared brain regions implicated in reward-guided decision making and learning in humans and monkeys, and attempted to identify their key subdivisions in relation to function (Fig. 1). We used fMRI in 25 monkeys and 38 humans to delineate the functional interactions of "decision-making regions" with other areas in the brain while subjects were at rest. Such interactions are reliant on anatomical connections between areas (15) and determine the information an area has access to and the way it can influence other areas, and thereby behavior. Each region of the brain has a defining set of interactions, a connectional or interactional "finger-print" (16), that can be compared across species (17–19). We focused on areas throughout the entire medial and orbital frontal lobe, including the ACC, lOFC, vmPFC, and frontal pole (FP) that have been related to decision making in humans and monkeys. The results suggested areal correspondences between species, as well as finer functional fractionations within regions than previously assumed. In a second step we used a complementary technique, diffusion-weighted (DW) MRI, to confirm the existence of 21 distinct component regions within the human medial and orbitofrontal cortex. The results suggest that every day human decision making capitalizes on a neural apparatus similar to that supporting decision making in monkeys.

Significance

Because of the interest in reward-guided learning and decision making, these neural mechanisms have been studied in both humans and monkeys. But whether and how key brain areas correspond between the two species has been uncertain. Areas in the two species can be compared as a function of the brain circuits in which they participate, which can be estimated from patterns of correlation in brain activity measured with functional MRI. Taking such measurements in 38 humans and 25 macaques, we identified fundamental similarities between the species and one human frontal area with no monkey counterpart. Altogether these findings suggest that everyday human decision-making capitalizes on a neural apparatus similar to the one that supports monkeys when foraging in the wild.

Author contributions: F.-X.N. and M.F.S.R. designed research; F.-X.N. and R.B.M. performed research; R.B.M. and J.S. contributed new reagents/analytic tools; F.-X.N. and R.B.M. analyzed data; and F.-X.N., R.B.M., and M.F.S.R. wrote the paper.

The authors declare no conflict of interest.

This article is a PNAS Direct Submission.

Freely available online through the PNAS open access option.

[1]To whom correspondence should be addressed. Email: franz-xaver.neubert@psy.ox.ac.uk.

This article contains supporting information online at www.pnas.org/lookup/suppl/doi:10.1073/pnas.1410767112/-/DCSupplemental.

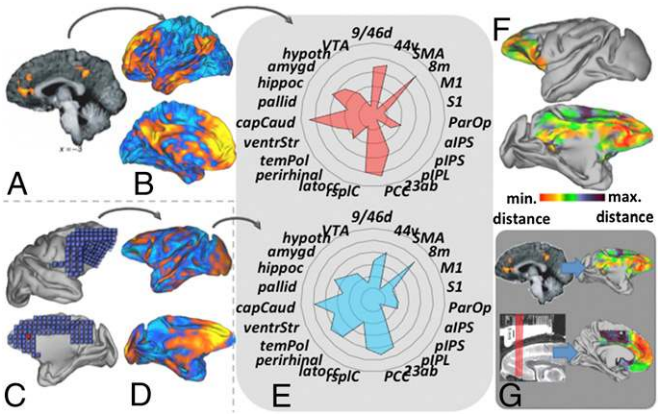

Fig. 1. (*A*) Overall approach of the study. fMRI analyses in 38 humans and 25 macaques were used to establish the whole-brain functional connectivity of regions in medial and orbital frontal cortex identified with reward-guided learning and decision making in the two species. The example shows the macaque brain regions that have a similar coupling profile to a human vmPFC region identified in a decision-making study (27). Reproduced from ref. 27, with permission from Macmillan Publishers Ltd, Nature Neuroscience. (*B*) Each region's functional connectivity with 23 key regions was then determined and (*C*) summarized as a functional connectivity fingerprint. (*D*) Once the functional connectivity fingerprint of a human brain area was established it was compared with the functional connectivity fingerprints of 380 ROIs in macaque orbital and medial frontal cortex (one example is shown here) by calculating the summed absolute difference [the "Manhattan" or "city-block" distance (17–19) of the coupling scores]. (*E*) Examples of the functional connectivity fingerprints for a human (blue) and a monkey (red) brain area. Most monkey ROIs matched human areas relatively poorly and extremely good and extremely bad matches were relatively rare. We used two SDs below the mean of this distribution of summed absolute differences as a cut-off to look for "significantly" good human to monkey matches. (*F*) A heat map summarizing the degree of correspondence between the functional connectivity patterns of each voxel in the macaque and the human brain region shown in *A*. Warm red areas indicate macaque voxels that correspond most strongly. (*G*) Complementary parts of the investigation started with the functional connectivity fingerprints of both human (*Upper*) and macaque (*Lower*) brain areas involved in reward-guided learning and decision making and then compared them with the functional connectivity fingerprints of areas in the other species. (*Top Left*) Reproduced from ref. 27, with permission from Macmillan Publishers Ltd, Nature Neuroscience. (*Bottom Left*) Reproduced from ref. 11, with permission from Macmillan Publishers Ltd, Nature Neuroscience.

Results

The first goal was to relate human frontal cortical regions implicated in decision making and learning in neuroimaging studies to monkey brain regions (Fig. 1*F*). We also did the reverse; we identified human brain regions resembling monkey frontal cortical regions implicated in decision making and learning.

We took the following approach: each time we looked at a specific human region we compared its functional coupling pattern to those associated with a set of 448 different monkey regions of interest (ROIs) within the ACC, lOFC, vmPFC, and FP trying to find one that would constitute the closest monkey match to the human region. We represented the closeness of the match at each voxel as a heat map. In most analyses several warm regions were apparent in the map but in each case the hottest area was found in an orbital or medial frontal region and it was this region that was taken as the best candidate for interspecies correspondence and highlighted with an arrow in Figs. 2–5. Notably, the other warm areas in the map tended to be ones with which the frontal area being investigated was connected; in other words, the approach identified areas in similar functional circuits in the other species but in each case it particularly highlighted one potential homolog in the frontal cortex. We also did the reverse by matching monkey regions to 417 different human ROIs trying to find the best human match for any given monkey area. The comparisons were based on the frontal regions' activity coupling with 23 cortical and subcortical ROIs already identified as comparable in the two species (*SI Appendix*, Table S2).

VmPFC, Perigenual ACC, and Subgenual ACC. Human vmPFC activity has been linked to subjective values of objects and choices (20–22). Positive correlation between activity and the values of chosen options and negative correlations with values of rejected options suggests a role in decision making (21) or attentional selection (23). However, there is also evidence the vmPFC tracks values of items even in the absence of any decision or when watching somebody else choosing (24, 25). Some studies have suggested that these value representations are independent of reward type (money, food) (26) and reflect the impact of other

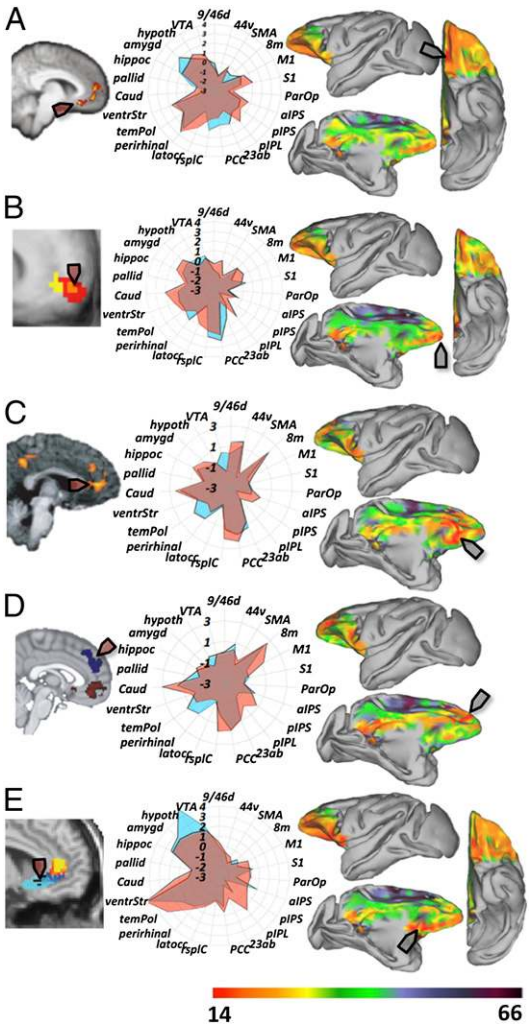

Fig. 2. Human medial frontal regions (*Left*) linked with (*A*) reward-guided decision making (21), (*B*) more abstract reward-guided decision making (28), (*C*) cost-benefit valuation (27), (*D*) imagining the reward outcomes of others (40), and (*E*) self-valuation and depression (42), could all be linked to macaque brain regions (*Right*) via similarities in their coupling patterns (*Center*: blue, macaque; red, human). However, a human brain area (*D*) associated with reward outcome imagination did not correspond in a simple way with any area in the macaque. (*A*) Reproduced from ref. 21, with permission from Elsevier. (*B*) Reproduced from ref. 28, with permission from Macmillan Publishers Ltd, Nature Neuroscience. (*C*) Reproduced from ref. 27, with permission from Macmillan Publishers Ltd, Nature Neuroscience. (*D*) Modified from ref. 40. (*E*) Modified from ref. 42.

factors affecting valuation, such as delay (27), indicating a "common currency" value representation. However, other studies have hinted at a posterior-to-anterior gradient of increasing abstractness in value representation (28). Here we show that this diversity of activity patterns is a consequence of the existence of several distinct component regions within the human vmPFC that can each be linked to different regions in the macaque.

We took the peak Montreal Neurological Institute (MNI) coordinates from a study implicating the vmPFC in decision making (21) and established its functional coupling pattern in humans (Fig. 2*A*). Similar activations have been reported nearby (10, 29, 30). The vmPFC had positive functional coupling with the OFC, retrosplenial, lateral occipital, inferior temporal, posterior temporo-parietal junction (TPJp), and perirhinal cortex, as well as considerable coupling with the amygdala, hypothalamus, and ventral striatum. However, it is negatively coupled with the lateral FP (FPl) cortex, ACC, and midinferior parietal lobule (IPL). A similar coupling pattern was seen when we took a coordinate from a food valuation task reported by McNamee et al. (28). A coupling pattern very similar to this was found in the monkey on the medial gyrus rectus near area 14m, as defined by Mackey and Petrides (31).

We next examined the coupling pattern associated with a more anterior vmPFC region implicated especially in representing values of abstract goods and choices (28) (Fig. 2*B*). Like adjacent regions, it exhibited some degree of coupling with the amygdala, hypothalamus, ventral striatum, medial temporal cortex, and temporal pole, but had stronger coupling with the posterior cingulate cortex (PCC), precuneus, and the head of the caudate. This area did not show negative coupling with the FPl, but instead with the supplementary motor area (SMA), pre-SMA, M1, and the intraparietal sulcus (IPS). This region's fMRI coupling pattern matched that of the monkey's anterior gyrus rectus and FP in areas 11m and 10m (31, 32).

We looked at a region identified by Kable and Glimcher (27) (Fig. 2*C*) that has activity that closely tracks the subjective values of delayed monetary rewards. The region is more dorsal and closer to the genu of the corpus callosum than the value-comparison regions discussed so far (Fig. 2 *A* and *B*). One suggestion is that it has a more direct role in tracking values rather than in making value-guided decisions (33–36). This region's coupling pattern was also distinct. Although it coupled with the temporal pole and TPJp, it also coupled with the PCC, precuneus, dorsolateral PFC (dlPFC), FPl, and the head of the caudate. The region correlates negatively with the SMA, dorsal premotor area (PMd), M1, and IPS. In a further analysis, we examined an even more dorsal perigenual region linked to individual variation in cost-benefit decision making (figure 4d in ref. 10, and in the supplementary information in ref. 37), and found that it was associated with a similar pattern of coupling (*SI Appendix*, Fig. S1*A*), although now there was less coupling with medial temporal regions, such as the amygdala and with dorsal and ventrolateral PFC and more coupling with premotor areas, such as the SMA. Voxels with similar coupling patterns were also found in the macaque in an arc of the perigenual cortex corresponding to cingulate area 24 and perhaps part of area 32 (38). It is interesting to note that another region showing high similarity is in retrosplenial areas 30 and 29, which reflects the fact that regions that are connected, as is the case for the perigenual ACC (pgACC) and retrosplenial cortex (39), tend to have similar connections with other regions across the brain. Importantly, the best-matching area of human pgACC is macaque area pgACC.

This region is not identical with the one previously mentioned to be related to value-comparison in the vmPFC. We formally tested the region's coupling patterns for significant differences using permutation testing and cluster-mass thresholding (*SI Appendix*, Fig. S7*A*). We established that, whereas the vmPFC is more strongly coupled with the OFC, and inferior temporal and temporal pole areas, the pgACC was more strongly coupled with the posterior cingulate and retrosplenial cortex. These significant differences were largely similar across species and are consistent with the notion that these regions have different roles to play in value representation and reward-guided decision making (33–36).

Activity has also been reported in a more dorsal and anterior region (35). Nicolle et al. (40) reported activity here when subjects were asked to imagine what values delayed monetary rewards would have for another person (*SI Appendix*, Fig. S2*D*). A similar region was active when people imagined how much they would like new and unexperienced food items that were nevertheless composed of familiar components (30). The resting fMRI coupling pattern associated with this region resembled that associated with the two perigenual regions reported by Kable and Glimcher (27) and Kolling et al. (10, 37) (Fig. 2*E*); however, the comparative weakness of coupling with the amygdala and temporal cortex areas meant that it most closely resembled a swathe of tissue in the macaque that extended from the anterior cingulate sulcus through area 9 on the dorsal convexity to the principal sulcus. These dorsomedial prefrontal cortex areas (dmPFC) can be reliably dissociated from vmPFC areas. We conducted a formal test for significant differences (*SI Appendix*, Fig. S7*B*) in coupling patterns between the dmPFC (areas 32d and 9 from the connectivity-based parcellation, see below) and vmPFC (areas 14m and 11m). The dmPFC was significantly more coupled with cingulate motor areas (CMA), pre-SMA, dlPFC, and posterior ventrolateral PFC (vlPFC), as well as the head of the caudate, whereas the vmPFC was significantly more coupled with other parts of the OFC, inferior temporal and lateral occipital, as well as precuneus and ventral striatum. These significant differences were largely similar across species.

Another more posterior and subgenual vmPFC region is implicated in the altered pattern of self-valuation associated with depression (41) (Fig. 2*E*). This area is the target of deep brain stimulation in patients with treatment-resistant depression (42). We looked at the coupling pattern of this region and found it resembled other vmPFC regions; it shared strong positive functional coupling with the OFC, posterior inferior temporal, and perirhinal cortex but had stronger coupling with the ventral striatum, amygdala, and hypothalamus. In addition, this area had strong coupling with the medial temporal cortex and temporal pole. It was strongly negatively coupled with the FPl, dlPFC, and dmPFC. A similar coupling pattern was observed in the monkey in subgenual cingulate voxels in area 25 (31). This region's coupling pattern, however, could be distinguished from that of the more anterior vmPFC identified with value-comparison and decision making. When a formal statistical comparison of the coupling patterns associated with these regions in the mid-vmPFC and subgenual vmPFC (Fig. 2 *A* and *B*) was made, it was clear that there was a significant difference (*SI Appendix*, Fig. S8*A*). Moreover, a three-way comparison of the subgenual vmPFC, anterior vmPFC, and pgACC confirmed that all three regions were robustly separable (*SI Appendix*, Fig. S8*B*).

Next, we wanted to relate areas identified in macaques back to the human frontal cortex (Fig. 3). Only a small number of studies have recorded this area of the macaque brain. Monosov and Hikosaka (5) report two subregions in the macaque vmPFC: a ventral subregion contained neurons persistently more active when monkeys experienced appetitive stimuli and a more dorsal subregion was more active when monkeys perceived aversive stimuli or "punishment." By establishing the functional coupling of these two adjacent monkey vmPFC subregions, we were able to match them, respectively, to a more antero-ventral (Fig. 3*A*) and a more postero-dorsal region within human vmPFC (Fig. 3*B*). The coupling patterns associated with the more antero-ventral region resembled the region linked to simple value-guided choices (Fig. 2*A*), whereas the coupling pattern associated with the postero-dorsal area resembled that associated with the subgenual region linked to altered self-valuation and depression (Fig. 2*D*).

Amemori and Graybiel (11) have reported neurons in a dorsal perigenual cingulate region that play an important role in cost-

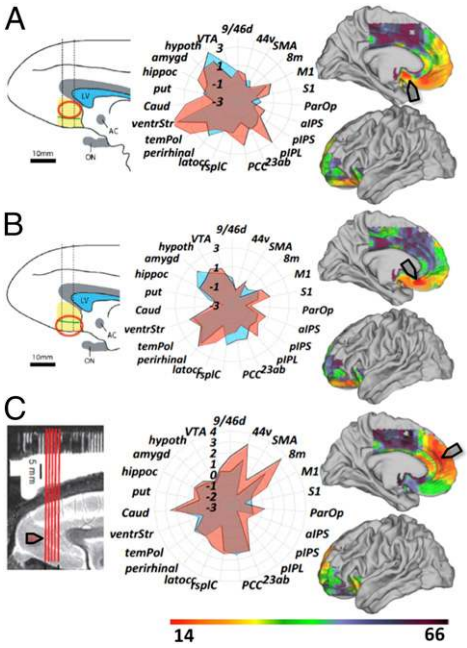

Fig. 3. Macaque medial frontal regions (*Left*) associated with (*A*) positive reward expectations (5), (*B*) negative outcome expectations (5), and (*C*) cost-benefit decision making (11) could all be linked to human brain regions (*Right*) via similarities in their coupling patterns (*Center*). (*A* and *B*) Reproduced from ref. 5. (*C*) Modified from ref. 11, with permission from Macmillan Publishers Ltd, Nature Neuroscience.

benefit decision making. The fMRI coupling pattern associated with this region was distinct to that associated with the areas studied by Monosov and Hikosaka (5), but it resembled to some degree that associated with voxels in human dorsal perigenual cingulate cortex (Fig. 3*C*) near regions implicated in cost-benefit integration in humans (27) (Fig. 2*C*), especially the more dorsal ones studied by Kolling et al. (10, 37) (*SI Appendix*, Fig. S1*A*).

Dorsal ACC. The dorsal ACC has been linked with executive control, inhibition, task switching, conflict resolution, and motor planning (13, 43–45). Here we tried to establish whether a so-called "task-positive" region in the human ACC (13) (Fig. 4*A*) could be found in the monkey ACC. In humans, this region is consistently "active" in several different cognitive control tasks and activity recorded here is sometimes referred to as being in the posterior rostral cingulate zone (RCZp) (46). Based on its strong coupling with sensorimotor areas (M1, S1, SMA, pre-SMA, PMd, PMv), areas in the IPS (anterior IPS, and posterior IPS), moderate coupling with the dlPFC, and strong negative coupling with temporal lobe areas (TPJp, temporal pole, and superior temporal sulcus), we were able to match it to a monkey ACC region. This region was located in the middle of the cingulate sulcus close to the ventral CMA (CMAv) (47).

Other human neuroimaging studies have implicated the ACC in learning and updating values of choices (48–50). Activity in this region is sometimes described as being in the anterior RCZ (RCZa) (46) (Fig. 4*B*). This region's strong positive functional coupling with the dlPFC, parietal operculum, insula, and pallidum, and strong negative coupling with the vmPFC, ventral striatum, amygdala, posterior IPL, and temporal lobe areas made it similar to a monkey region in the anterior cingulate sulcus near the rostral CMA (CMAr) (47).

Both of these ACC regions, the RCZa/CMAr (Fig. 4*B*) and RCZp/CMAv (Fig. 4*A*), had quite distinct coupling patterns to the pgACC regions discussed in the previous section (Figs. 2*C* and 3*C*). In addition, they were distinct to other even more posterior ACC regions that correspond to the caudal cingulate zone/dorsal cingulate motor area (CCZ/CMAd) and to more ventral parts of area 23a (area 23/ab) (*SI Appendix*, Fig. S2). This finding was confirmed with a formal statistical comparison between these three region's coupling patterns (*SI Appendix*, Fig. S9*A*). However, the three cingulate motor areas, CCZ, RCZp, and RCZa, also shared fundamental similarities in their coupling patterns: all three showed some degree of coupling with the pre-SMA, SMA, dlPFC, and premotor, as well as anterior, IPL caudate and putamen. We looked for a significant gradient of change in functional coupling from anterior to posterior cingulate motor regions and showed that moving anteriorly increased coupling with the dlPFC and parts of vlFC and insula, whereas moving posteriorly led to increased coupling with the PCC and precuneus, sensorimotor, and parietal regions (*SI Appendix*, Fig. S9*B*). Finally, another statistical comparison between the coupling patterns associated with the RCZa/CMAr, RCZp/CMAv, and pgACC further confirmed the existence of differences in coupling between the most anterior cingulate motor area and the dorsal part of the pgACC (*SI Appendix*, Fig. S9*C*).

Finally, we sought to identify human brain regions resembling the ACC region in which neurons have been recorded that encode reward prediction errors (51, 52) (Fig. 4*C*). This region most closely resembled the human RCZa (Fig. 4*B*).

OFC and FP. In macaques, neurons in the medial orbital sulcus in central OFC have been associated with context-independent value representation (53), whereas the lOFC has been associated with credit assignment (54). There is also evidence of a link between human lOFC and credit assignment (55). Human FPl has been implicated in coding the value or relevance of alternative choices

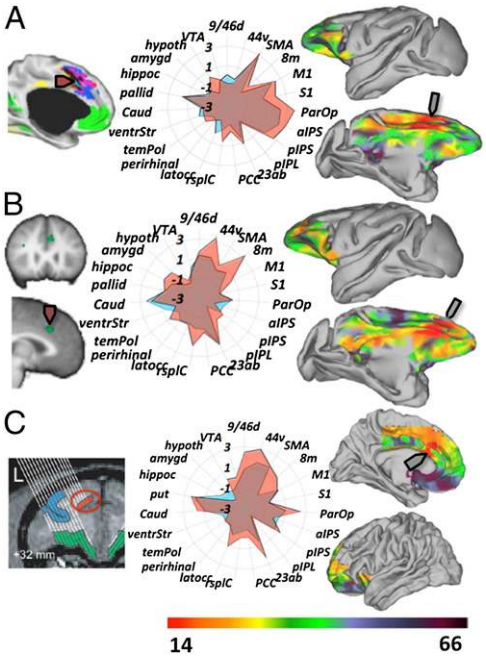

Fig. 4. Human ACC regions (*Left*) linked with (*A*) cognitive control (13) and (*B*) reward-guided action selection and behavioral updating (49) could be linked to macaque brain regions (*Right*) via similarities in their coupling patterns (*Center*). (*C*) A macaque ACC region (*Left*) linked with reward-guided behavioral updating (51) could be linked to a similar human ACC region to that shown in *B*. (*A*) Modified from ref. 13, with permission from Elsevier. (*B*) Reproduced from ref. 49, with permission from Macmillan Publishers Ltd, Nature Neuroscience. (*C*) Reproduced from ref. 49, with permission from Macmillan Publishers Ltd, Nature Neuroscience.

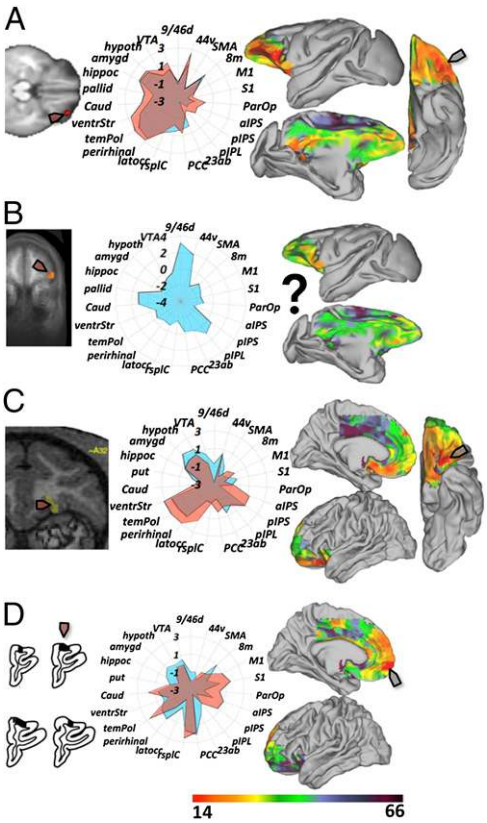

Fig. 5. Human OFC regions (*Left*) linked with (*A*) stimulus-reward association (55) and could be linked to a macaque lOFC (*Right*) via similarities in the regions' coupling patterns (*Center*). (*B*) A human brain concerned with decision-making under ambiguity (61) did not correspond strongly to any macaque brain region. (*C* and *D*) Macaque regions (*Left*) linked with (*C*) context-independent and outcome identity-dependent value signals (53) and (*D*) decision outcome monitoring (63) could be linked to human brain regions (*Right*) via similarities in coupling patterns (*Center*). (*A*) Reproduced from ref. 55. (*B*) Modified from ref. 61. (*C*) Reproduced from ref. 53, with permission from Macmillan Publishers Ltd, Nature Neuroscience. (*D*) Modified from ref. 63, with permission from Macmillan Publishers Ltd, Nature Neuroscience.

or strategies that are not pursued at the moment but which might be in the near future (8).

We attempted to match human posterior lOFC and anterior lOFC/FP regions with regions in the monkey. There has been particular interest in the possibility that human lOFC, especially the posterior lOFC, is important when adverse outcomes, including punishment, lead to behavioral change (33, 56). However, it has proved difficult to identify a particular region of macaque OFC in which neurons are specialized for responding to punishment, and instead reward-related neurons have been found across the medial-lateral extent of the OFC (57–59). One possibility is that there is a major difference between human and macaque OFC, but an alternative hypothesis is that the lOFC, even in humans, is not just concerned with punishing outcomes but that it is concerned with using any outcome, positive or negative, to guide behavioral change. For example, positive outcomes might lead to behavioral changes in learning situations. Consistent with this idea, some recent studies have suggested that the same lOFC region previously highlighted as responsive to punishers (33, 56) has a more general role in credit assignment and the linking of stimuli to reward outcomes (55, 60) (Fig. 5*A*). In contrast, more anterior lOFC areas in humans are active during decision making under ambiguity (61) (Fig. 5*B*).

The human posterior lOFC region was, in terms of its strong positive functional coupling with the vmPFC, ventrolateral PF (vlFC), ventral striatum, and temporal cortex, and its negative coupling with the ACC, sensorimotor, and parietal areas, most similar to a region in the monkey lOFC. Such a correspondence is consistent with this region being concerned with the mediation of behavioral change as a result of a general role in learning stimulus-reward associations (55, 60, 62). However, we were unable to match the more anterior human lOFC region linked to ambiguity (Fig. 5*B*), which positively coupled with the mid-IPL, FPl, and dlPFC, and negatively coupled with the ACC, vmPFC, precuneus, ventral striatum, and temporal cortex, to any of the 448 ROIs in the monkey frontal cortex. Formal statistical comparisons of the coupling patterns associated with human anterior and posterior lOFC confirmed the existence of differences in both species (*SI Appendix*, Fig. S10*A*).

Next, we sought human regions corresponding to areas investigated in the macaque. Neurons in the monkey medial orbitofrontal sulcus encode context-invariant values of goods (53). This region showed strong positive coupling with the rest of the OFC, regions in the temporal lobes (temporal pole, parts of the hippocampus, superior and inferior temporal gyri, perirhinal cortex), lateral occipital cortex, and ventral striatum, and negative coupling with sensorimotor areas and premotor areas (Fig. 5*C*). It matched a region with a similar coupling profile in the posterior part of the human central OFC. This part of the human brain is not the same as the more medial vmPFC regions that have been the focus of investigations of value encoding in the human brain (Fig. 2), but it is similar to a region in which activity has been related to the identity of reward outcomes (60). In this central OFC region, unlike in the lOFC, activity is related to the identities of rewards rather than the association between rewards and predictive cues. We conducted a formal statistical comparison between the coupling patterns of a vmPFC/medial OFC region and a lateral OFC region (*SI Appendix*, Fig. S10*B*). This comparison confirmed significant differences between these two regions, which have previously been linked with processing of positive and negative outcomes (33) or value comparison and credit assignment (8), respectively. Statistical comparisons of the coupling patterns associated with the vmPFC (Fig. 2*A*), central

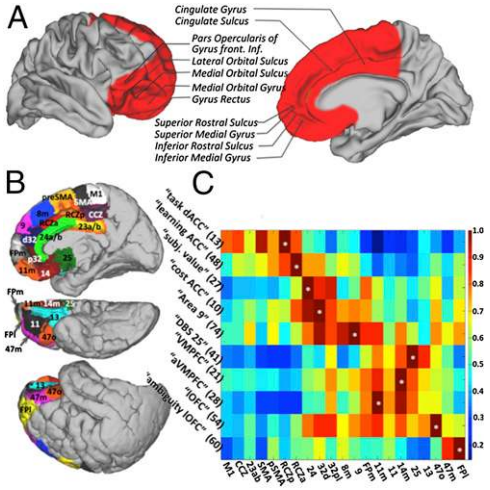

Fig. 6. (*A*) The human medial and orbital region investigated and (*B*) the subregions that could be identified on the basis of differences in DW-MRI–estimated connectivity. (*C*) Correspondences between the fMRI-based functional coupling maps associated with decision-making areas (Figs. 1–5) and orbital and medial subregions identified via DW-MRI parcellation (*B*). Warm red colors indicate similarities in the functional coupling maps and asterisks indicate areas with highest spatial correlation (see *SI Appendix, Section 5* for more information).

OFC (Fig. 5*C*), and lateral OFC (Fig. 5*A*) confirmed that they each participated in different neural circuits in both species (*SI Appendix*, Fig. S12*A*). This finding suggests that there are not only important differences between the vmPFC/medial OFC and lateral OFC (33, 56), but that a central OFC region is also distinct.

A region in monkey FP (Fig. 5*D*) implicated in linking choices with their outcomes (63) exhibited strong positive coupling with the PCC, hippocampus, temporal pole, and head of the caudate, and negative correlation with the cingulate motor areas, insula, and IPS (Fig. 4*D*). It therefore matched a region in human FPm.

DW-MRI Parcellation of Medial and Orbital Frontal Cortical Areas for Decision Making. So far, our comparison of fMRI coupling patterns in macaques and humans has suggested several correspondences, but it has also suggested a more fine-grained fractionation of the vmPFC, OFC, ACC, and FP than is often assumed. In the next part of our investigation, a different imaging modality and analysis approach, DW-MRI tractography, was used to provide an independent test of the parcellation of the human frontal cortex suggested by the fMRI coupling pattern analysis.

DW-MRI can be used to estimate the structural connectivity of each MRI voxel and this information can then be used to group together voxels sharing similar profiles of connectivity with the rest of the brain (64). Despite the technique's limitations (65), the areas previously identified using the DW-MRI approach correspond in their spatial position to areas identified in cytoarchitectural analysis (19, 66–69). A previous parcellation of human ACC on the basis of DW-MRI tractography has been published (70), but the region investigated in that study excluded much of the vmPFC, all of the OFC, the area between the ACC and FP, and because it did not establish dorsal boundaries of ACC areas it left open the possibility of additional areas. Here we investigated a much larger ROI comprising the vmPFC, ACC, FP, and OFC in their entirety and extending into the adjacent PCC and dorsal frontal cortex.

We ran probabilistic tractography from each voxel in the ROI (Fig. 6*A*) in 38 right-handed human participants in both left and right hemispheres with and without paracingulate sulci. In general, the paracingulate sulcus is prominent in the left but not always in the right hemisphere (71), and so results are shown for the left hemisphere in cases with a paracingulate sulcus (Fig. 6*B*) and in the right hemisphere in cases lacking a paracingulate sulcus (*SI Appendix*, Fig. S3). The results were, however, broadly similar. We correlated the pattern of structural connectivity of every voxel in the ROI with all other voxels in the same ROI and obtained a symmetric cross-correlation matrix. We then used *k*-means clustering to group together voxels with similar connection patterns. We used this approach recursively, dividing the initial ROI into two smaller subdivisions and subsequently subdividing the resulting areas further in three to four parcellation steps. We stopped when results ceased being consistent across subjects. In a final step we returned to the fMRI data and established the functional coupling patterns of all of the DW-MRI parcellation-derived subregions and compared them with the coupling fingerprints of the functional areas investigated in the first part of the study (Fig. 6*C*) and with the 448 monkey frontal ROIs aiming to find the closest match for each (*SI Appendix*, Fig. S5).

We found five clusters in the dorsal ACC bordering medial aspects of M1, SMA, pre-SMA, and 8m [which were in turn also identified by this parcellation but were already discussed elsewhere (17)]. Three overlapped with clusters 4, 5, and 6 as proposed by Beckmann et al. (70) and which correspond to the areas Picard and Strick (46) call RCZa, RCZp, and CCZ (Fig. 6*B*, red, orange, and brown), with left hemisphere centers of gravity [−9, 20, 34], [−8, 7, 40], and [−11, −26, 42], respectively. The functional coupling patterns of the RCZa and RCZp resembled coupling patterns of the two cingulate areas in the first part of the study (Fig. 4). More ventrally, we delineated two regions that, together, overlapped with Beckmann et al.'s (70) cluster 7. These were termed 23a/b and 24a/b (Fig. 6*B*, green and dark-yellow) with centers of gravity [−4, 19, 23] and [−6, −15, 35]. These regions were coupled to each other, to the premotor cortex and SMA, to the IPL, and to some degree with the dlPFC and with negative coupling with temporal lobe areas (*SI Appendix*, Fig. S4). There was a posterior-to-anterior gradient of decreasing sensorimotor and pallidal coupling and increasing dlPFC and caudate head coupling. Similar coupling patterns are found for monkey cingulate gyrus areas, such as 24 and 23d (*SI Appendix*, Fig. S4) (72). The functional coupling pattern of the more anterior part of 24 suggested a correspondence with the pgACC area (27) implicated in cost-benefit decision making (Figs. 3*C* and 6*C*).

More anteriorly, on the medial surface we delineated seven clusters (Fig. 6*B*). A subgenual area (Fig. 6*B*, green) overlapped with Beckmann et al.'s (70) cluster 1 and the region described by Johansen-Berg et al. (42) as a deep brain stimulation target site in depression. The area's center of gravity [−4, 5, −8] suggested correspondence with area 25 (31). Two further clusters lay in the vmPFC. The center of gravity [−9, 23, −19] of the more rostral area (Fig. 6*C*, orange) suggested a resemblance with area 11m (31). The more posterior overlapped in position with Beckmann et al.'s (70) cluster 2 (Fig. 6*B*, dark-red) and its center of gravity [−9, 23, −18] linked it to area 14m (31). The fMRI coupling patterns of these two regions indicated correspondence with vmPFC decision-making regions (Fig. 6*C*; compare with Fig. 2 *A* and *B*). We identified two regions (Fig. 6*B*, dark blue and dark red) with centers of gravity [−9, 36, 28] and [−11, 47, 4] suggesting correspondences with subdivisions of area 32: d32 and p32 (73). The fMRI coupling pattern associated with the more dorsal of these, area d32, resembled the coupling pattern of the dorsal pgACC area linked to cost-benefit decision making during foraging (10). A medial area 9 and a medial FP cluster were also found (Fig. 6*B*, pink and gray) that overlapped with area 9 identified by Sallet et al. (17) and FPm identified by Neubert et al. (19) at [−10, 51, 29] and [−11, 60, 4]. Area 9's coupling pattern resembled that of the area linked to imagination of other peoples' values and unexperienced rewards (30, 40) (Fig. 6*C* and *SI Appendix*, Fig. S1). The FPm's functional coupling pattern was similar to the monkey FP region investigated by Tsujimoto et al. (63) (Figs. 5*D* and 6*C*).

On the lateral surface, we delineated three clusters (Fig. 6*B*, yellow, pink, and orange) with centers of gravity at [−31, 50, 60], [−30, 50, −8], and [−32, 24, −11], which we relate to FPl (19, 69), and two distinct components of area 47/12 we refer to as 47/12m (anterior) and 47/12o (posterior), respectively (31). FPl, which resembled the ambiguity area described by Levy et al. (61) (Figs. 5*B* and 6*C*), exhibited little correspondence with areas in the macaque brain (19). Area 47/12m exhibited only a limited degree of correspondence with macaque 47/12. Area 47/12o, which resembled the lOFC region concerned with credit assignment (55) (Figs. 5*A* and 6*C*), resembled the posterior part of 47/12 in macaque.

Next we divided the central part of the OFC into areas corresponding to clusters 2 and 3 of Kahnt et al. (74) (Fig. 6*B*, bright blue and black) with centers of gravity at [−13, 22, −21] and [−22, 30, −17]. These two central OFC areas had very distinct coupling patterns: the posterior region showed strong positive coupling with the ventrolateral frontal cortex, vmPFC, perirhinal cortex, the temporal pole, amygdala, and the ventral striatum, and so resembled area 13 in the macaque (31) and the region studied by Padoa-Schioppa and Assad (53). In contrast, the more anterior OFC region, which we refer to as 11, coupled strongly with regions such as the dlPFC, vlPFC, vmPFC, temporal pole, and ventral striatum, and resembles a monkey anterior central OFC region.

In a final set of analyses we sought to investigate whether the human brain areas in the cingulate and OFC that we identified and the macaque brain areas we identified as homologous occupy a similar position within the brain networks of the two

species (see also *SI Appendix*, *Section 4*). First, we calculated the dissimilarity matrices of all 23 study and parcellation-derived homologous frontal regions with one another within each species and performed a correlation between the two species' matrices. The two dissimilarity measures were highly correlated between species ($\rho = 0.79$, $P < 0.001$). Second, we calculated two measures of the centrality of the medial and orbital frontal regions within the network of target areas. Centrality measures indicate how important a node is within a network. Again, the correlations between species in these measures were highly significant (degree centrality: $\rho = 0.57$, $P = 0.005$; eigenvector centrality: $\rho = 0.56$, $P = 0.005$). Third, to provide another line of evidence regarding the "relational similarity" of the frontal areas under investigation, we performed a hierarchical clustering analysis for both species on the whole-brain functional coupling of all areas derived from the tractography-based parcellation of the human medial and orbital cortex (*SI Appendix*, Fig. S13*A*) and their proposed monkey equivalents (*SI Appendix*, Fig. S13*B*). The hierarchical clustering analyses did not reveal identical relationships between areas in the two species when they were examined at the finest level, but it can be seen that at the broader level clustering into families of regions is largely similar across species. Five broad groups of areas are identifiable in both species: (*i*) the cingulate motor areas, (*ii*) the perigenual and medial frontopolar regions, (*iii*) the vmPFC and anterior central OFC regions, (*iv*) the posterior medial and central OFC regions, and (*v*) the lateral OFC. This finding supports the idea that despite fine-grained differences between species, it is possible to identify broad similarities in the way that frontal areas interact in circuits in the two species.

Discussion

Despite its apparent sophistication, human reward-guided decision making and learning appears to depend on medial and orbital frontal cortical circuits that are similar to ones that can be identified in macaques. Moreover, careful inspection of the patterns of interregional interaction revealed a finer level of parcellation between component areas within the ACC, vmPFC, and OFC than is often assumed in decision-making investigations.

In a previous study of the parietal cortex it was shown that areas with distinctive DW-MRI–estimated connectivity profiles corresponded to distinct cytoarchitectural regions (66–68). Although DW-MRI investigation is no substitute for more detailed investigation of cytoarchitecture, it may guide such investigations and it provides information about the approximate extent of anatomical areas on a scale that corresponds with the majority of human neuroimaging studies. Human vmPFC is one of the most frequently reported areas of activity in investigations of reward-guided decision-making, but it was possible to show that this area consists of subregions, each exhibiting a distinctive pattern of activity coupling with the rest of the brain. Moreover, in most cases the regions were associated with distinctive DW-MRI–estimated connectivity profiles.

A region near area 14m has been linked to decisions or attentional selection of choices (21, 23, 29, 30). In comparison with the ACC and OFC it was, in both species, distinguished by strong positive coupling with hypothalamus, ventral striatum, and amygdala (75). Reward-related activity has been reported in a similar area in the macaque (5) and lesions here disrupt reward-guided decision making (76). Two more anterior areas, 11m and 11, were linked with more abstract choices (28), but they nevertheless bore a resemblance to areas 11m and 11 in the macaque (31). In monkeys lesions that include area 11 and area 13 disrupt decision making guided by contrasts in outcome identity and reward-specific satiety, and not just reward amount (77).

In monkeys, neurons in the central OFC encode the value of a specific item, regardless of the value of the other items with which it is presented (53). The functional coupling of this region resembled that of a part of the human central OFC, area 13, but it was different to the more medial vmPFC areas that have been the focus of investigations of value representations in the human brain (Fig. 1). The coupling did, however, correspond to the human region identified by Klein-Flügge et al. (60) as coding reward identity. This pattern of results is broadly consistent with the scheme suggested by Rudebeck and Murray (78), in which value-based decisions and reward identity-based decisions are mediated by medial and central orbital regions, respectively. As discussed below, however, an even more lateral OFC region can be distinguished that is concerned with establishing stimulus–reward associations and credit assignment (54, 55, 60).

A dorsal medial frontal area in humans, area 9, was linked to decision making when the outcome had to be imagined or modeled in some way (30, 40), and its activity coupling pattern resembled area 9 (79) in the monkey medial frontal cortex. A slightly more ventral area, d32, resembled the region active when decisions have to be made about whether rewards are worth the cost of foraging (10). Although it has been argued that no exact homolog of human d32 exists in the macaque (73), it was notable that its activity coupling pattern resembled that seen in the dorsal part of macaque area 32, which is in the anterior cingulate sulcus, a region sometimes called 32(s) (80). A region with a similar coupling pattern in the monkey has also been associated with cost-benefit decision making (11). The coupling pattern for this region could be distinguished from, but nevertheless resembled, a distinct region, pgACC, that is active when participants trade magnitudes of rewards against their respective delays (27). This cost-benefit comparison or derivation of a "common currency" appears to be a distinct process to the comparison of values associated with different choices to make a decision; this latter process is associated with more ventral parts of the medial surface in areas 11m and 14m (Figs. 2, 3, and 6, and *SI Appendix*, Fig. S1).

Human d32 and monkey 32(s) are very distinct in their coupling patterns from more posterior dorsal ACC areas that have also been implicated in decision making, learning, and cognitive control. The more anterior RCZa/CMAr is responsive to feedback about motor strategies, especially when this is relevant to changes of behavior in the future both in humans (10, 43, 49, 50, 81) and macaques (51, 82). This region seems more active whenever there is evidence that the current mode of action is suboptimal and alternative behaviors should be considered. The strong positive coupling of RCZa with areas involved in cognitive control—such as the dlPFC, supramarginal gyrus, pre-SMA, inferior frontal gyrus, and subthalamic nucleus—might support this function of seeking for alternative behavioral strategies. The more posterior RCZp area has been called a task-positive region that is active in situations of conflict (83), when subjects need to engage in various different tasks (13) or during low-frequency responding (43). Generally speaking, this area seems to be more active whenever there is a higher demand placed on motor control, be it conflict, effort, or infrequent motor behavior. The area's strong coupling with sensorimotor areas (M1), IPS, and areas that have been implicated in top-down motor control (SMA, PMd, ventral premotor area) might support this function. One might think of the different role of RCZp and RCZa as paralleling the role of areas 45 and 47/12: whereas area 45 seems to select certain objects and visual features for attention (84), the more anterior area 47/12 might be more involved in learning new visual objects–reward associations (8). RCZp and RCZa might do something similar in the action domain: whereas RCZp might help selecting and attending specific motor plans, RCZa might acquire evidence for switching behavioral strategies away from the current mode of action.

A correspondence was identified between the lOFC area 47/12o in macaques and humans. In contrast to the medial OFC and vmPFC and central OFC, monkey lOFC is necessary for associating specific outcomes with specific choices (54). Simi-

larly, in humans it is more active in situations when specific rewards can be associated with specific outcomes (55, 60). Its coupling pattern–strong positive correlation with vlFC, middle and inferior temporal lobe areas, as well as the perirhinal cortex, would put this area in an excellent position to access visual information of varying degrees of abstractness, whereas its strong coupling with the ventral striatum, amygdala, and the vmPFC link it with reward and value-guided choice networks. The area is therefore ideally placed for credit assignment and learning about which sensory features in the environment are rewarding.

When decisions have to be made in highly ambiguous situations, a more anterior lOFC/FPl region tends to be active (61, 85). Moreover, the FPl has been proposed to track values of alternative choices (21, 37) and stores information about alternative strategies or task sets when they should not be used at the moment but might be returned to later (86, 87). In short, this region shows activity correlated with the number of alternative options, strategies, and task sets, or the amount of evidence that alternative options might be worth pursuing. This would put the area in a good position to signal uncertainty about the effectiveness of our current behavior, and therefore allow critical evaluation and metarepresentation of our decisions (88). The FPl coupled strongly with the mid-IPL, dlPFC, and pre-SMA and was not matched to any monkey ROI. Note that the functional coupling pattern of human FPl was largely different from the coupling pattern of monkey FPm, as described by Tsujimoto et al. (63). Our results suggest that Tsujimoto et al. (63) recorded from an area more similar to human FPm.

The similarity in areas' coupling patterns between species provides a strong case that these areas perform similar functions in the two species. This theory is further demonstrated by the comparison of different measures of the positions that the cingulate and orbitofrontal regions occupy within the larger brain network. The coupling with predefined target regions, the different measures of the centrality of the areas, and the grouping of areas into subnetworks based on their whole-brain functional connectivity all provide evidence for a largely conserved organization of decision making areas in these two primates.

To conclude, the fMRI coupling patterns of areas in the medial and orbital frontal cortex in humans and macaques suggest that several meaningful subdivisions can be identified even within areas, such as the vmPFC, that are often treated as unitary. Moreover, many correspondences can be identified between the species although they are not always those that are widely assumed. A small number of areas may be found only in humans and not in macaques.

Methods

Human Participants. Resting-state blood-oxygen level-dependent fMRI (rs-fMRI) and DW and T1-weighted structural images were acquired in 38 healthy right-handed (according to Edinburgh Handedness Inventory: mean ± SD, 0.84 ± 0.19) participants (20 female; age range: 20–45 y; mean age ± SD, 30.7 ± 10.1 y) on a 3T Siemens Magnetom Verio MR scanner in the same session using standard DW-MRI and rs-fMRI protocols (*SI Appendix, Section 1*). All participants gave written informed consent in accordance with ethical approval from the Oxford Research Ethics Committee. Participants lay supine in the scanner and cushions were used to reduce head motion. Participants were instructed to lie still and keep their eyes open and fixated at a cross. Twelve participants had no paracingulate sulcus in their left hemisphere (noparacingulate_left), 20 had a prominent paracingulate sulcus in their left hemisphere (paracingulate_left), and 22 had no paracingulate sulcus in their right hemisphere (noparacingulate_right). For both the rs-fMRI based functional coupling analyses and the DW-tractography–based parcellation, we calculated group results for the two most common patterns (paracingulate_left; noparacingulate_right), trying to establish whether any interindividual differences could be explained by the two factors hemisphere (left vs. right) or paracingulate sulcus (prominently present or absent). Both DW-tractography–based parcellation and rs-fMRI results yielded largely similar results for all subjects.

Human rs-fMRI Data Acquisition, Preprocessing, and Analysis. Analyses were performed using tools from FSL (Functional MRI of the Brain Software Library), the Human Connectome Project Workbench, and custom-made software written in Matlab (MathWorks). rs-fMRI data acquisition and preprocessing were carried out in a standard way, as previously described (66) (*SI Appendix, Section 1*). To establish the functional connectivity of each region, we created ROIs based on exemplary functional imaging studies with human participants that related a specific aspect of decision making to "activity" in a circumscribed part of one of these areas (*SI Appendix*, Table S1). We drew a cubic ROI (3 × 3 × 3 voxels; i.e., 6-mm isotropic) centered on the peak MNI coordinate of a given study. These ROIs were registered from MNI-space to each subject's individual rs-fMRI space via the T1-weighted structural image using FNIRT and brain boundary-based registration. Then the major Eigen time series representing activity in each of the ROIs was calculated.

Individual statistical maps were then calculated using a seed-based correlation analysis, which is part of FSL (fsl_sbca), as previously described (66, 89), to infer the functional connectivity of these ROIs with the rest of the brain. For each ROI we created a model consisting of the first Eigen time series of that region and the confounding time series representing head movement (six regressors resulting from motion correction using MCFLIRT) and the Eigen time-series of white-matter and corticospinal fluid. The results of each individual subject's ROI-specific seed-based correlation analysis were then entered into a general linear model analysis. The resulting *z*-statistical images were projected onto the CaretBrain as provided by the Human Connectome Project Workbench using the "surf_proj" algorithm as implemented in FSL, and then visualized using the Human Connectome Project Workbench. Unthresholded *z*-maps were quantified by extracting the average intensity of each ROI's functional connectivity *z*-map in a number of cortical and subcortical regions of interest that we refer to as target regions to distinguish them from the orbital and medial frontal regions that were the focus of our investigation (*SI Appendix*, Table S2). These regions were chosen, first, because they are known to be interconnected with particular orbital and medial frontal regions in the macaque and so the functional connectivity patterns of different orbital and medial frontal areas are likely to be distinguishable on the basis of their coupling with these areas. Second, the areas were chosen because their homology in humans and macaques has already been established. We drew ROIs (3 × 3 × 3 voxels; i.e., 6-mm isotropic) centered on the coordinates listed in *SI Appendix*, Table S2 and then averaged the *z*-value from the unthresholded seed-based correlation analysis derived *z*-maps within these ROIs. These values were then displayed on a spider plot (Figs. 1–5). On the basis of these coupling fingerprints, the human decision-making areas were then compared with 448 different ROIs in the monkey frontal cortex to establish the monkey ROI with the most similar coupling pattern (see below). Note that the spider plots illustrate the simple correlation between a frontal lobe area and the target areas as opposed to partial correlations because: (*i*) It makes the link between the spider plots and the functional connectivity *z*-maps in Figs. 1–5 transparent. (*ii*) It prevents underestimation of the coupling between a frontal area and a target area if they are both also coupled to a second target area (recall that the target areas were chosen because they were likely to be connected to the frontal areas being investigated). Comparisons between the coupling patterns of different frontal areas to a given target area become transparent even if only one of the frontal areas and the target area being examined are both coupled to another target area. (*iii*) It ensures that judgments about similarities in the coupling patterns of frontal areas in humans and macaques are not influenced by interspecies differences in the way that target areas are interconnected with one another. However, it is important to remember that although it is the case that such coupling patterns reflect monosynaptic connections, they do not do so exclusively (15). In addition, a complementary analysis based on partial correlation is shown in *SI Appendix*, Fig. S6.

In another analysis, monkey regions from different neurophysiological recording studies were compared, based on their functional coupling patterns, to 417 ROIs in the human frontal cortex. These 417 different ROIs (3 × 3 × 3 voxels; i.e., 6-mm isotropic) were drawn in equal distance to one another (6 mm) to cover the medial and orbital frontal and frontopolar cortex. The region covered everything that has been referred to as the ACC, OFC or FP (Fig. 5*A*). It therefore comprised the whole region investigated by Beckmann et al. (70), except the two most posterior clusters (8, 9). The region included the cingulate gyrus and sulcus (including the dorsal bank of the paracingulate sulcus if present) and extended posteriorly to include all cingulate motor areas as delineated by Beckmann et al. (70) and Amiez and Petrides (90). Therefore, the region covered the most anterior tip of the marginal sulcus but excluded the precuneus and PCC. Anteriorly, the region included the subgenual ACC and vmPFC. Moreover, it contained areas 9,

FPm, and FPl, as delineated by Neubert et al. (19) and Sallet et al. (17), the OFC, and the orbital part of the inferior frontal gyrus (pars orbitalis gyri frontalis inferioris). These 417 different ROIs were then registered from MNI-space to each subject's individual rs-fMRI space. To infer the functional connectivity of these 417 ROIs with the rest of the brain, we used exactly the same procedure as described above for the decision-making study-based ROIs. In this way we were able to obtain 417 different group *z*-statistical images that were subsequently used to generate 417 different coupling fingerprints, using exactly the same 23 cortical and subcortical target ROIs as mentioned above. These 417 different coupling fingerprints could then be compared with each of the monkey areas from neurophysiological recording studies (see below).

Macaque rs-fMRI Data Acquisition, Preprocessing, and Analysis. rs-fMRI and anatomical scans were collected for 25 healthy macaques (*Macaca mulatta*) (four females, age: 3.9 y, weight: 5.08 kg) under light inhalational anesthesia with isoflurane (for detailed information on anesthesia protocol, monitoring of vital signs, data acquisition, and preprocessing, see *SI Appendix, Section 2*). Protocols for animal care, MRI, and anesthesia were performed under authority of personal and project licenses in accordance with the United Kingdom Animals (Scientific Procedures) Act (1986).

The goal of this part of the study was to test for similarities between the functional networks of areas implicated in decision making in human and monkey frontal cortex. We therefore aimed to map the resting-state functional connectivity networks of areas derived from exemplary neurophysiological recording studies of macaque monkeys, which had related neuronal activity measures to specific aspects of decision making. We drew cubic ROIs (3-mm isotropic) centered on the center of gravity of the recording site of each study. These ROIs were registered from standard-space to each monkey's individual rs-fMRI space using FNIRT. Then the major Eigen time series representing activity in each of the ROIs was calculated and seed-based correlation analysis (fsl_sbca) was used, as in the human subjects, to infer the functional connectivity of these ROIs with the rest of the brain. As in the human subjects, unthresholded group *z*-maps were quantified by extracting the average intensity of each ROI's functional connectivity *z*-map with 23 cortical and subcortical target regions of interest (*SI Appendix*, Table S2). These coupling fingerprints of monkey "decision-making areas" were then compared with 417 different ROIs in the human orbital and medial frontal cortex to establish regions with the best corresponding functional coupling pattern (see below).

For the reverse comparison (matching human neuroimaging-derived decision-making regions to areas in the monkey frontal cortex), we drew 448 equally spaced cubic ROIs (3-mm isotropic) to cover the whole cingulate gyrus and sulcus, as well as areas 9, 10, 12, 45, 47/12, 14, 11, 13, and Iai, as defined by ref. 32. These 448 different ROIs were then registered from standard-space to each monkey's individual rs-fMRI space using FNIRT. To infer the functional connectivity of these 448 ROIs with the rest of the brain, we used exactly the same fsl_sbca-based procedure as described above. In this way we were able to obtain 448 different group *z*-statistical images which were again used to generate 448 different coupling fingerprints using exactly the same 23 cortical and subcortical target areas as mentioned above. These 448 different coupling fingerprints could then be compared with each of the human areas from neuroimaging studies (see below). We also conducted DW-tractography–based parcellation of the same orbital and medial frontal region (Fig. 5*A*) in our human participants (see below) and matched the functional coupling profiles of each of the different parcels to these 448 monkey ROIs using the same coupling fingerprint matching approach.

Comparison of Resting-State Functional Connectivity of Macaque and Human Decision-Making Areas. A formal comparison between human and macaque coupling patterns was performed by calculating the summed absolute difference [the "Manhattan" or "city-block" distance (17–19) of the coupling scores]. This process yielded a summary measure of the difference in coupling patterns for each pair of areas in the two species (e.g., for human "task-positive ACC" compared with monkey ROI number 267 the summed absolute difference between coupling profiles is 34.78). The summary measure can then be used to compare the functional coupling pattern of each human region with those of all 448 regions in the macaque and vice versa. The Manhattan distance has previously been used to compare the coupling patterns of brain areas across species (17–19). It is a useful metric for comparing connectivity because it is summarizes the whole pattern of coupling for an area. It is the whole pattern of connectivity rather than any particular connection that distinguishes areas and so this metric is appropriate. In addition, unlike some other possible approaches, it is less sensitive to any idiosyncrasy in the estimate of any one connection. This summary measure was then back-projected onto the monkey brain for each of the 448 ROIs to show regions with low absolute difference in red and regions with high absolute difference in brown/black (Figs. 1–5). Thus, the right hand side of Figs. 2–5 can be thought of as "heat maps" in which warm red colors indicate the regions in the brain of one species that best correspond with the area highlighted from the other species on the left hand side.

DW-Tractography–Based Parcellation of Orbital and Medial Frontal ROI. DW-MRI data were preprocessed in a standard way, as previously described (66) (*SI Appendix, Sections 3 and 4*). For each participant, probabilistic tractography was run from each voxel in the orbital and medial frontal ROI (Fig. 6*A* and *SI Appendix*, Fig. 2*A*) in three groups (noparacingulate_right, noparacingulate_left, paracingulate_left) to assess connectivity with every brain voxel (whole-brain "target" was down-sampled after tractography to 5-mm isotropic voxels for the connectivity matrix to be manageable; however, the whole orbital and medial frontal ROI was tracked in original FA space, using a model accounting for multiple fiber orientations in each voxel. A connectivity matrix between all orbital and medial frontal voxels and every other brain voxel was derived and used to generate a symmetric cross-correlation matrix of dimensions (number of seeds × number of seeds) in which the (*i*, *j*) element value is the correlation between the connectivity profile of seed *i* and the connectivity profile of seed *j*. The rows of this cross-correlation matrix were then permuted using *k*-means segmentation for automated clustering to define different clusters (Fig. 6*B* and *SI Appendix*, Fig. 3). The goal of clustering the cross-correlation matrix is to group together seed voxels that share the same connectivity with the rest of the brain.

We used a recursive or iterative clustering procedure here similar to the one used by Beckmann et al. (70) and Neubert et al. (19). In this way, the orbital and medial ROI was parcellated into subregions via three to four parcellation steps. Parcellation was stopped when the resulting parcel could not be further subdivided in a similar way in all subjects into either two, three, or four subregions (with preference to two over three and three over four). A subdivision was considered reliable if the topography of the different clusters was the same in all subjects of a particular group (for example noparacingulate_left).

ACKNOWLEDGMENTS. This study was funded in part by the Medical Research Council UK (R.B.M., J.S., and M.F.S.R.); a Christopher Welsh scholarship at the University of Oxford (to F.-X.N.); a Netherlands Organisation for Scientific Research fellowship from the Dutch Organization for Scientific Research (to R.B.M.); and The Wellcome Trust (to J.S. and M.F.S.R.).

1. Wallis JD (2012) Cross-species studies of orbitofrontal cortex and value-based decision-making. *Nat Neurosci* 15(1):13–19.
2. Rangel A, Hare T (2010) Neural computations associated with goal-directed choice. *Curr Opin Neurobiol* 20(2):262–270.
3. O'Doherty JP (2011) Contributions of the ventromedial prefrontal cortex to goal-directed action selection. *Ann N Y Acad Sci* 1239:118–129.
4. Bouret S, Richmond BJ (2010) Ventromedial and orbital prefrontal neurons differentially encode internally and externally driven motivational values in monkeys. *J Neurosci* 30(25):8591–8601.
5. Monosov IE, Hikosaka O (2012) Regionally distinct processing of rewards and punishments by the primate ventromedial prefrontal cortex. *J Neurosci* 32(30):10318–10330.
6. Padoa-Schioppa C, Cai X (2011) The orbitofrontal cortex and the computation of subjective value: Consolidated concepts and new perspectives. *Ann N Y Acad Sci* 1239: 130–137.
7. Cole MW, Yeung N, Freiwald WA, Botvinick M (2009) Cingulate cortex: Diverging data from humans and monkeys. *Trends Neurosci* 32(11):566–574.
8. Rushworth MF, Noonan MP, Boorman ED, Walton ME, Behrens TE (2011) Frontal cortex and reward-guided learning and decision-making. *Neuron* 70(6):1054–1069.
9. Hare TA, Schultz W, Camerer CF, O'Doherty JP, Rangel A (2011) Transformation of stimulus value signals into motor commands during simple choice. *Proc Natl Acad Sci USA* 108(44):18120–18125.
10. Kolling N, Behrens TE, Mars RB, Rushworth MF (2012) Neural mechanisms of foraging. *Science* 336(6077):95–98.
11. Amemori K, Graybiel AM (2012) Localized microstimulation of primate pregenual cingulate cortex induces negative decision-making. *Nat Neurosci* 15(5):776–785.
12. Cai X, Padoa-Schioppa C (2012) Neuronal encoding of subjective value in dorsal and ventral anterior cingulate cortex. *J Neurosci* 32(11):3791–3808.
13. Dosenbach NU, et al. (2006) A core system for the implementation of task sets. *Neuron* 50(5):799–812.
14. Ridderinkhof KR, Ullsperger M, Crone EA, Nieuwenhuis S (2004) The role of the medial frontal cortex in cognitive control. *Science* 306(5695):443–447.
15. O'Reilly JX, et al. (2013) Causal effect of disconnection lesions on interhemispheric functional connectivity in rhesus monkeys. *Proc Natl Acad Sci USA* 110(34): 13982–13987.
16. Passingham RE, Stephan KE, Kötter R (2002) The anatomical basis of functional localization in the cortex. *Nat Rev Neurosci* 3(8):606–616.

17. Sallet J, et al. (2013) The organization of dorsal frontal cortex in humans and macaques. *J Neurosci* 33(30):12255–12274.
18. Mars RB, Sallet J, Neubert FX, Rushworth MF (2013) Connectivity profiles reveal the relationship between brain areas for social cognition in human and monkey temporoparietal cortex. *Proc Natl Acad Sci USA* 110(26):10806–10811.
19. Neubert FX, Mars RB, Thomas AG, Sallet J, Rushworth MF (2014) Comparison of human ventral frontal cortex areas for cognitive control and language with areas in monkey frontal cortex. *Neuron* 81(3):700–713.
20. Plassmann H, O'Doherty J, Rangel A (2007) Orbitofrontal cortex encodes willingness to pay in everyday economic transactions. *J Neurosci* 27(37):9984–9988.
21. Boorman ED, Behrens TE, Woolrich MW, Rushworth MF (2009) How green is the grass on the other side? Frontopolar cortex and the evidence in favor of alternative courses of action. *Neuron* 62(5):733–743.
22. Gläscher J, Hampton AN, O'Doherty JP (2009) Determining a role for ventromedial prefrontal cortex in encoding action-based value signals during reward-related decision making. *Cereb Cortex* 19(2):483–495.
23. Lim SL, O'Doherty JP, Rangel A (2011) The decision value computations in the vmPFC and striatum use a relative value code that is guided by visual attention. *J Neurosci* 31(37):13214–13223.
24. Lebreton M, Jorge S, Michel V, Thirion B, Pessiglione M (2009) An automatic valuation system in the human brain: Evidence from functional neuroimaging. *Neuron* 64(3):431–439.
25. Cooper JC, Kreps TA, Wiebe T, Pirkl T, Knutson B (2010) When giving is good: Ventromedial prefrontal cortex activation for others' intentions. *Neuron* 67(3):511–521.
26. Levy DJ, Glimcher PW (2011) Comparing apples and oranges: Using reward-specific and reward-general subjective value representation in the brain. *J Neurosci* 31(41):14693–14707.
27. Kable JW, Glimcher PW (2007) The neural correlates of subjective value during intertemporal choice. *Nat Neurosci* 10(12):1625–1633.
28. McNamee D, Rangel A, O'Doherty JP (2013) Category-dependent and category-independent goal-value codes in human ventromedial prefrontal cortex. *Nat Neurosci* 16(4):479–485.
29. De Martino B, Fleming SM, Garrett N, Dolan RJ (2013) Confidence in value-based choice. *Nat Neurosci* 16(1):105–110.
30. Barron HC, Dolan RJ, Behrens TE (2013) Online evaluation of novel choices by simultaneous representation of multiple memories. *Nat Neurosci* 16(10):1492–1498.
31. Mackey S, Petrides M (2010) Quantitative demonstration of comparable architectonic areas within the ventromedial and lateral orbital frontal cortex in the human and the macaque monkey brains. *Eur J Neurosci* 32(11):1940–1950.
32. Saleem KS, Logothetis NK (2007) *A Combined MRI and Histology Atlas of the Rhesus Monkey Brain in Stereotaxic Coordinates* (Academic, London; Burlington, MA), pp ix, 326 pp.
33. Grabenhorst F, Rolls ET (2011) Value, pleasure and choice in the ventral prefrontal cortex. *Trends Cogn Sci* 15(2):56–67.
34. Rolls ET, Grabenhorst F, Parris BA (2010) Neural systems underlying decisions about affective odors. *J Cogn Neurosci* 22(5):1069–1082.
35. Rolls ET, Grabenhorst F, Deco G (2010) Decision-making, errors, and confidence in the brain. *J Neurophysiol* 104(5):2359–2374.
36. Rolls ET, Grabenhorst F, Deco G (2010) Choice, difficulty, and confidence in the brain. *Neuroimage* 53(2):694–706.
37. Kolling N, Wittmann M, Rushworth MF (2014) Multiple neural mechanisms of decision making and their competition under changing risk pressure. *Neuron* 81(5):1190–1202.
38. Vogt BA, Vogt L, Farber NB, Bush G (2005) Architecture and neurocytology of monkey cingulate gyrus. *J Comp Neurol* 485(3):218–239.
39. Morecraft RJ, Cipolloni PB, Stilwell-Morecraft KS, Gedney MT, Pandya DN (2004) Cytoarchitecture and cortical connections of the posterior cingulate and adjacent somatosensory fields in the rhesus monkey. *J Comp Neurol* 469(1):37–69.
40. Nicolle A, et al. (2012) An agent independent axis for executed and modeled choice in medial prefrontal cortex. *Neuron* 75(6):1114–1121.
41. Murray EA, Wise SP, Drevets WC (2011) Localization of dysfunction in major depressive disorder: Prefrontal cortex and amygdala. *Biol Psychiatry* 69(12):e43–e54.
42. Johansen-Berg H, et al. (2008) Anatomical connectivity of the subgenual cingulate region targeted with deep brain stimulation for treatment-resistant depression. *Cereb Cortex* 18(6):1374–1383.
43. Braver TS, Barch DM, Gray JR, Molfese DL, Snyder A (2001) Anterior cingulate cortex and response conflict: effects of frequency, inhibition and errors. *Cereb Cortex* 11(9):825–836.
44. Duncan J, Owen AM (2000) Common regions of the human frontal lobe recruited by diverse cognitive demands. *Trends Neurosci* 23(10):475–483.
45. Frank MJ, Samanta J, Moustafa AA, Sherman SJ (2007) Hold your horses: Impulsivity, deep brain stimulation, and medication in parkinsonism. *Science* 318(5854):1309–1312.
46. Picard N, Strick PL (1996) Motor areas of the medial wall: A review of their location and functional activation. *Cereb Cortex* 6(3):342–353.
47. Dum RP, Strick PL (2002) Motor areas in the frontal lobe of the primate. *Physiol Behav* 77(4-5):677–682.
48. Walton ME, Devlin JT, Rushworth MFS (2004) Interactions between decision making and performance monitoring within prefrontal cortex. *Nat Neurosci* 7(11):1259–1265.
49. Behrens TE, Woolrich MW, Walton ME, Rushworth MF (2007) Learning the value of information in an uncertain world. *Nat Neurosci* 10(9):1214–1221.
50. O'Reilly JX, et al. (2013) Dissociable effects of surprise and model update in parietal and anterior cingulate cortex. *Proc Natl Acad Sci USA* 110(38):E3660–E3669.
51. Kennerley SW, Behrens TE, Wallis JD (2011) Double dissociation of value computations in orbitofrontal and anterior cingulate neurons. *Nat Neurosci* 14(12):1581–1589.
52. Matsumoto M, Matsumoto K, Abe H, Tanaka K (2007) Medial prefrontal cell activity signaling prediction errors of action values. *Nat Neurosci* 10(5):647–656.
53. Padoa-Schioppa C, Assad JA (2008) The representation of economic value in the orbitofrontal cortex is invariant for changes of menu. *Nat Neurosci* 11(1):95–102.
54. Walton ME, Behrens TE, Buckley MJ, Rudebeck PH, Rushworth MF (2010) Separable learning systems in the macaque brain and the role of orbitofrontal cortex in contingent learning. *Neuron* 65(6):927–939.
55. Noonan MP, Mars RB, Rushworth MF (2011) Distinct roles of three frontal cortical areas in reward-guided behavior. *J Neurosci* 31(40):14399–14412.
56. Kringelbach ML, Rolls ET (2004) The functional neuroanatomy of the human orbitofrontal cortex: Evidence from neuroimaging and neuropsychology. *Prog Neurobiol* 72(5):341–372.
57. Rolls ET (2008) Functions of the orbitofrontal and pregenual cingulate cortex in taste, olfaction, appetite and emotion. *Acta Physiol Hung* 95(2):131–164.
58. Morrison SE, Salzman CD (2009) The convergence of information about rewarding and aversive stimuli in single neurons. *J Neurosci* 29(37):11471–11483.
59. Rich EL, Wallis JD (2014) Medial-lateral organization of the orbitofrontal cortex. *J Cogn Neurosci* 26(7):1347–1362.
60. Klein-Flügge MC, Barron HC, Brodersen KH, Dolan RJ, Behrens TE (2013) Segregated encoding of reward-identity and stimulus-reward associations in human orbitofrontal cortex. *J Neurosci* 33(7):3202–3211.
61. Levy I, Snell J, Nelson AJ, Rustichini A, Glimcher PW (2010) Neural representation of subjective value under risk and ambiguity. *J Neurophysiol* 103(2):1036–1047.
62. Noonan MP, et al. (2010) Separate value comparison and learning mechanisms in macaque medial and lateral orbitofrontal cortex. *Proc Natl Acad Sci USA* 107(47):20547–20552.
63. Tsujimoto S, Genovesio A, Wise SP (2010) Evaluating self-generated decisions in frontal pole cortex of monkeys. *Nat Neurosci* 13(1):120–126.
64. Johansen-Berg H, et al. (2004) Changes in connectivity profiles define functionally distinct regions in human medial frontal cortex. *Proc Natl Acad Sci USA* 101(36):13335–13340.
65. Johansen-Berg H, Rushworth MF (2009) Using diffusion imaging to study human connectional anatomy. *Annu Rev Neurosci* 32:75–94.
66. Mars RB, et al. (2011) Diffusion-weighted imaging tractography-based parcellation of the human parietal cortex and comparison with human and macaque resting-state functional connectivity. *J Neurosci* 31(11):4087–4100.
67. Scheperjans F, et al. (2008) Probabilistic maps, morphometry, and variability of cytoarchitectonic areas in the human superior parietal cortex. *Cereb Cortex* 18(9):2141–2157.
68. Caspers S, et al. (2008) The human inferior parietal lobule in stereotaxic space. *Brain Struct Funct* 212(6):481–495.
69. Bludau S, et al. (2014) Cytoarchitecture, probability maps and functions of the human frontal pole. *Neuroimage* 93(Pt 2):260–275.
70. Beckmann M, Johansen-Berg H, Rushworth MF (2009) Connectivity-based parcellation of human cingulate cortex and its relation to functional specialization. *J Neurosci* 29(4):1175–1190.
71. Paus T, et al. (1996) Human cingulate and paracingulate sulci: Pattern, variability, asymmetry, and probabilistic map. *Cereb Cortex* 6(2):207–214.
72. Vogt BA, Nimchinsky EA, Vogt LJ, Hof PR (1995) Human cingulate cortex: Surface features, flat maps, and cytoarchitecture. *J Comp Neurol* 359(3):490–506.
73. Vogt BA, et al. (2013) Cingulate area 32 homologies in mouse, rat, macaque and human: Cytoarchitecture and receptor architecture. *J Comp Neurol* 521(18):4189–4204.
74. Kahnt T, Chang LJ, Park SQ, Heinzle J, Haynes JD (2012) Connectivity-based parcellation of the human orbitofrontal cortex. *J Neurosci* 32(18):6240–6250.
75. Ongür D, Price JL (2000) The organization of networks within the orbital and medial prefrontal cortex of rats, monkeys and humans. *Cereb Cortex* 10(3):206–219.
76. Noonan MP, Sallet J, Rudebeck PH, Buckley MJ, Rushworth MF (2010) Does the medial orbitofrontal cortex have a role in social valuation? *Eur J Neurosci* 31(12):2341–2351.
77. Rudebeck PH, Murray EA (2011) Dissociable effects of subtotal lesions within the macaque orbital prefrontal cortex on reward-guided behavior. *J Neurosci* 31(29):10569–10578.
78. Rudebeck PH, Murray EA (2011) Balkanizing the primate orbitofrontal cortex: Distinct subregions for comparing and contrasting values. *Ann N Y Acad Sci* 1239:1–13.
79. Petrides M, Pandya DN (1999) Dorsolateral prefrontal cortex: Comparative cytoarchitectonic analysis in the human and the macaque brain and corticocortical connection patterns. *Eur J Neurosci* 11(3):1011–1036.
80. Morecraft RJ, et al. (2012) Cytoarchitecture and cortical connections of the anterior cingulate and adjacent somatomotor fields in the rhesus monkey. *Brain Res Bull* 87(4-5):457–497.
81. Walton ME, Bannerman DM, Alterescu K, Rushworth MFS (2003) Functional specialization within medial frontal cortex of the anterior cingulate for evaluating effort-related decisions. *J Neurosci* 23(16):6475–6479.
82. Kennerley SW, Walton ME, Behrens TE, Buckley MJ, Rushworth MF (2006) Optimal decision making and the anterior cingulate cortex. *Nat Neurosci* 9(7):940–947.
83. Kerns JG, et al. (2004) Anterior cingulate conflict monitoring and adjustments in control. *Science* 303(5660):1023–1026.
84. Nelissen N, Stokes M, Nobre AC, Rushworth MF (2013) Frontal and parietal cortical interactions with distributed visual representations during selective attention and action selection. *J Neurosci* 33(42):16443–16458.
85. Yoshida W, Ishii S (2006) Resolution of uncertainty in prefrontal cortex. *Neuron* 50(5):781–789.
86. Koechlin E, Hyafil A (2007) Anterior prefrontal function and the limits of human decision-making. *Science* 318(5850):594–598.
87. Volman I, Roelofs K, Koch S, Verhagen L, Toni I (2011) Anterior prefrontal cortex inhibition impairs control over social emotional actions. *Curr Biol* 21(20):1766–1770.
88. Fleming SM, Weil RS, Nagy Z, Dolan RJ, Rees G (2010) Relating introspective accuracy to individual differences in brain structure. *Science* 329(5998):1541–1543.
89. O'Reilly JX, Beckmann CF, Tomassini V, Ramnani N, Johansen-Berg H (2010) Distinct and overlapping functional zones in the cerebellum defined by resting state functional connectivity. *Cereb Cortex* 20(4):953–965.
90. Amiez C, Petrides M (2012) Neuroimaging evidence of the anatomo-functional organization of the human cingulate motor areas. *Cereb Cortex* 24(3):563–578.